Analytical Methods

Accepted Manuscript

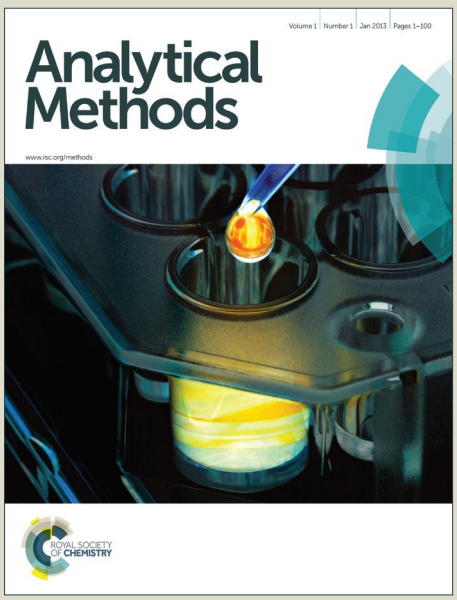

This is an *Accepted Manuscript*, which has been through the Royal Society of Chemistry peer review process and has been accepted for publication.

Accepted Manuscripts are published online shortly after acceptance, before technical editing, formatting and proof reading. Using this free service, authors can make their results available to the community, in citable form, before we publish the edited article. We will replace this *Accepted Manuscript* with the edited and formatted *Advance Article* as soon as it is available.

You can find more information about *Accepted Manuscripts* in the Information for Authors.

Please note that technical editing may introduce minor changes to the text and/or graphics, which may alter content. The journal's standard Terms & Conditions and the Ethical guidelines still apply. In no event shall the Royal Society of Chemistry be held responsible for any errors or omissions in this *Accepted Manuscript* or any consequences arising from the use of any information it contains.

ROYAL SOCIETY OF CHEMISTRY

www.rsc.org/methods

Journal Name

ARTICLE

Core-shell Fructus Broussonetiae-like Au@Ag@Pt nanoparticles as highly efficient peroxidase mimetics for supersensitive resonance-enhanced Raman sensing

Received 00th January 20xx,
Accepted 00th January 20xx

DOI: 10.1039/x0xx00000x

www.rsc.org/

Junrong Li, Liang Lv, Guannan Zhang, Xiaodong Zhou, Aiguo Shen* and Jiming Hu*

We herein present a simple and surfactant-free synthetic strategy to prepare core-shell Fructus Broussonetiae-like Au@Ag@Pt nanoparticles (FBNPs) via concerted actions of both galvanic replacement and reagent reduction, in which the chitosan (CS)-mediated epitaxial growth of Pt multi-branches occurs on the cresyl violet (CV) labeled Au core Ag shell nanoparticles (NPs) at room temperature. The as-prepared novel nanostructures possess intriguing enzyme mimetic activity due to the formation of Frucus Broussonetiae-shaped Pt shell, the absence of surfactants and the positively charged CS molecules intertwined within the outermost Pt NPs. Relying on the high sensitivity of resonance-enhanced Raman scattering (RRS) and the highly efficient intrinsic peroxidase-like activity of FBNPs, H_2O_2 was detected with a wider detection window from 10 pM to 100 μM when utilizing 3, 3', 5, 5'-tetramethylbenzidine (TMB) as substrates. It is exactly based on a H_2O_2-TMB catalytic oxidation system that a simple, sensitive, selective and universal platform has been reasonably extended for detection of all peroxidase-related analytes. Glucose with a concentration range (1 nM-200 μM), for example, has been detected in the presence of glucose oxidase (GOx) with a limit of detection of 1 nM.

1 Introduction

Since the first report on magnetite nanoparticles (NPs) [1] that possess the intrinsic enzyme mimetic activity similar to what natural peroxidase has, the synthesis and applications of these artificial enzyme mimetics have been developed by leaps and bounds. Many peroxidase mimetics, including Au@Pt@Au NPs[2], $CoFe_2O_4$ NPs[3, 4], nickel oxide[5], gold nanohybrids[6] and copper sulfide nanorods[7], have been widely investigated. Unfortunately, some of the catalysts may suffer from limited catalytic performance and complex synthetic routes while others show low suspending stability and nonuniform size. Therefore, attempts should be made to synthesize nanomaterial with high peroxidase mimic activity and satisfying physical character. In general, an ideal candidate to be proposed as peroxidase mimetics should satisfy the following characteristics[8-12]: (1) highly catalytic activity; (2) facile and surfactant-free synthetic approach; (3) uniform size and shape of nanostructures with high surface area; (4) high physical stability and monodispersity.

Among all the peroxidase candidates, one of the most extensively explored artificial enzymes is Platinum (Pt) contained[13, 14]. If not for the skyrocketing price and scarcity of Pt, these Pt-based peroxidase mimetics will have a broader use in practice. Therefore, how to reduce the amount of Pt in the currently used Pt nano-catalysts has been a consideration for the researchers[15, 16]. There is an effective and less costly method to substitute sectional Pt with Au[9, 10, 17] or Ag[18] in order to synthesize artificial enzyme mimetics that maintain efficient enzyme mimetic activity while exhibiting unique optical, electronic and thermal properties as well. The bimetallic Pt-based nanomaterials, especially for the Au cores decorated with Pt multi-branches, are competent to act as peroxidase mimetics maybe because they encompass the following merits[15, 16]: the higher performance of catalytic ability deriving from Pt multi-branches; the better chemical stability and durability stemming from Au cores; and the lower costs owing to the partial replacement of Pt with Au. Admittedly, various shapes of multi-branched Au@Pt NPs, such as nano-urchins[19] and nano-dendrites[20], have been synthesized, but some of these methods need large amounts of surfactants[21], high temperature[19, 21] and a narrow size distribution can't be guaranteed[22] while others require complicated multi-step synthesis[21]. For example, the tedious post-treatment processes have to be conducted to remove the surfactant from the surface of the nano-catalysts in order to obtain desirable catalytic activity. Up to date, it is still unavailable to synthesize a highly efficient Pt-contained peroxidase mimetic by using a simple and surfactant-free approach under mild conditions.

Typically, peroxidase mimetics are often employed to catalyze the oxidation of substrates in the presence of H_2O_2, followed by the change of chemical structures of substrates. The widely accepted substrates include 3, 3', 5, 5'-

Key Laboratory of Analytical Chemistry for Biology and Medicine (Ministry of Education), College of Chemistry and Molecular Sciences, Wuhan University Wuhan,430072, China. E-mail: agshen@whu.edu.cn; jmhu@whu.edu.cn
†Electronic Supplementary Information (ESI) available: See DOI: 10.1039/x0xx00000x

tetramethylbenzidine (TMB)[23], 2, 2'-azinobis 3-ethylbenzothiazoline-6-sulfonic acid (ABTS)[24] and o-phenylenediamine (OPD)[18], of which TMB enjoys a more popularity because it is less toxic and more sensitive than alternative substrates[25]. A universal strategy to detect H_2O_2 and the related substances can be established with the assistance of peroxidase mimetics considering the quantitative relationships between H_2O_2 and the oxidized substrates. To illustrate, combined glucose oxidase (GOx) with peroxidase mimetics, a rapid, convenient and reliable glucose sensor can be realized with the aid of intermediate H_2O_2 [8, 26, 27]. Normally, researchers regard UV-*vis* spectroscopy[23] as a common method to measure the absorption at 652 nm of the oxidized substrates. The absorption band at 652 nm may be assigned to charge transfer complex (CTC), which could be analyzed by RRS with 632.8 nm excitation[25]. Thus, surface-enhanced Raman scattering (SERS) resonance-enhanced Raman scattering (RRS), which is able to guarantee a more satisfying sensitivity, could be exploited as a new method of detection and quantification of the universal platform[28]. Utilizing the H_2O_2-TMB system, efforts in our group have been made to detect H_2O_2[29] and melamine[30] by taking advantage of RRS and surface-enhanced resonance Raman scattering (SERRS), respectively. Similar works have been done by other researchers. For example, Faulds et al. [31] firstly investigated the peroxidase-like activity of silver NPs and successfully realized the detection of H_2O_2 in a novel way. Cong and Jung et al.[32] fabricated a dual-biomimetic functional array containing both superhydrophobic and peroxidase-like activities. High sensitive detection of H_2O_2 was achieved by combining the bi-functional array and SERS. Nevertheless, reproducibility in RRS, SERS and SERRS quantitative analysis should arouse our concern in view of the signal fluctuations brought by the outer environment and instrumental factors. Thus, introduction of internal standards has become a focus among researchers to correct the signal fluctuation[33-36]. Compared with the internal standards appearing in the outside of the NPs, studies have shown that the signal fluctuations can be corrected remarkably by the internal standards embedded inside the shell, because the signals of the internal standards will not be influenced by the detection environment[37]. Therefore, quantifications related to Raman spectroscopy are encouraged to use nanomaterials with internal standards embedded inside the shell.

In this work, we report a simple and convenient strategy for high yield synthesis of well-dispersed and size-controlled core-shell Fructus Broussonetiae-like Au@Ag@Pt nanoparticles (FBNPs). The novel NPs encompass highly efficient peroxidase activity because the formation of Frucus Broussonetiae-shaped Pt shell, the absence of surfactants and the positively charged property. Combined the high sensitivity of RRS and the highly efficient intrinsic peroxidase-like activity of FBNPs, H_2O_2 was detected with a wide detection window from 10 pM to 100 μM. Based on the universal H_2O_2-TMB catalytic system, glucose was successfully detected with the limit of detection of 1 nM and the concentration range from 1 nM to 200 μM. More importantly, cresyl violet (CV), locating between Au core and Pt shell and thus freeing from the disturbance of the outer environment, was also adopted as the internal standards to correct the signal fluctuations.

2 Experimental sections

2.1 Materials

Hydrogen tetrachloroaurate (III) trihydrate ($HAuCl_4 \cdot 4H_2O$), dihydrogen hexachloroplatinate (IV) hexahydrate ($H_2PtCl_6 \cdot 6H_2O$), cresyl violet (CV) and sodium citrate were purchased from Sigma. Ascorbic acid (AA), silver nitrate, H_2O_2 (30 wt%), glucose, lactose and maltose were purchased from Sinopharm Chemical Reagent Co., Ltd. All the above chemicals were analytical reagent grade and used without further purification. Chitosan (CS) was purchased from Aladdin (deacetylated: 95%, viscosity: 100-200 mPa s). 3, 3', 5, 5'-tetramethylbenzidine (TMB) (BR) was purchased from Shanghai kayou Biological Technology Co., Ltd. Human serum samples were provided by the hospital of Wuhan University (Wuhan, China). Ultrapure water with an electrical resistance larger than 18.2 MΩ cm was used throughout the experiment.

2.2 Synthesis of FBNPs

Au NPs with a diameter of about 30 nm were prepared by reduction of $HAuCl_4$ with sodium citrate according to our previous research[38]. The Au NPs were used as seeds. Then, Au@Ag core-shell NPs were also prepared according to our previously reported method[39].

Au@Ag@CS core-shell NPs were prepared based on Au@Ag NPs. 12 μL of the CV solution (1mM), acting as the internal standard molecules of Raman signals, was added to 3 mL of Au@Ag core-shell NPs under stirring, followed by adding 1 mL of CS solution (0.1 mg/mL) immediately. Afterwards, the solution was mixed by ultrasonic for 15 min.

FBNPs were formed as follows: First, 4 mL of Au@Ag@CS NPs were mixed with 600 μL of AA (0.1 M). Then, H_2PtCl_6 (1 mM) was dropwise added into the mixture under stirring. The mixture was kept stirring for 15 min. The stripping of Ag shell and growth of Pt multi-branches shell was evidenced by the color change from orange to purple and finally brown. Before characterization and further applications, the FBNPs were centrifuged at 3000 rpm for 15 min and the supernatant was discarded. The precipitate was dispersed in ultrapure water.

2.3 Optimization of experimental conditions

(1) The amounts of H_2PtCl_6: three kinds of FBNPs were prepared with 1200 μL, 1800 μL and 2400 μL of H_2PtCl_6 (1 mM), respectively. 150 μL of TMB (5 mM), 20 μL of H_2O_2 (5 mM), 630μL of acetate buffer (pH 4.0) and 200μL of FBNPs were added into a 2 mL tube. The solution was incubated at 45°C water bath for 5 min and terminated in an ice-water bath for 10 min; (2) The amounts of FBNPs: after confirming the suitable amounts of H_2PtCl_6 was 1800 μL, the following steps were similar with (1) only by changing the volume of FBNPs

from 25 μL to 350 μL while using acetate buffer to keep the whole volume of the system constant; (3) pH: under the optimum condition of (1) and (2), the pH of acetate buffer was changed from 2 to 9; (4) Temperature: the temperature of incubation was tuned from 25°C to 60°C while keeping other parameters at the optimum value.

2.4 H_2O_2 detection using peroxidase mimetics (FBNPs)

150 μL of TMB (5 mM) and 20 μL of H_2O_2 were mixed in the reaction volume of 630 μL of acetate buffer (pH 4.0). Then, 200 μL of FBNPs were added subsequently. The mixed solution was incubated at 45°C water bath for 5 min, followed by keeping in an ice-water bath for 10 min terminating the reaction. The resulted reaction solution was subjected to Raman measurements.

2.5 Glucose detection using GOx and peroxidase mimetics (FBNPs)

(1) 20 μL of 5.0 mg/mL GOx and 200 μL of glucose with different concentrations in 10 mM phosphate buffered saline (PBS) (pH 7.4) were incubated at 37°C water bath for 15 min; (2) the above 20 μL of glucose solution, 150 μL of 5 mM TMB, 200 μL of FBNPs were added to 630 μL of 0.2 M acetate buffer (pH 4.0); (3) the mixed solution was incubated in a 45°C water bath for 5 min; (4) the resulted solution was immersed into an ice-water bath for 10 min terminating the reaction and used for Raman measurements afterwards.

In control experiments, three similar and separate assays took place using 100 μM maltose, lactose and fructose instead of glucose.

2.6. Kinetic analysis

The reaction kinetics for the catalytic oxidation of TMB was conducted by recording the absorption spectra at 652 nm within a 1 min interval using UV-*vis* spectrophotometer (Shimadzu, UV-2550). The reaction was conducted at 45°C with 200 μL of the as-prepared NPs in 630 μL of 0.2 M acetate buffer (pH 4) in the presence of different concentrations of TMB or H_2O_2. The apparent kinetic parameters were calculated according to Michaelis-Menten equation:

$$v = \frac{V_{max} \times [S]}{K_m + [S]}$$

Where v is the initial velocity, V_{max} is the maximal reaction velocity, K_{max} is the Michaelis constant and [S] is the concentration of substrate.

2.7 Characterization

A UV-*vis* spectrophotometer (Shimadzu, UV-2550) was used to record the absorption spectra of different reaction solutions. Raman measurements were performed with a confocal microscope (Jobin-Yvon HR-800). He-Ne Laser at 632.8 nm was used for excitation. Spectra were collected with 50 long working distance lens. The signal was integrated for 10 s twice accumulations. Zeta potentials were measured on a Nano-ZSP zetasier (Malvern Instruments). Scanning Electron Microscope images were obtained with a Scanning Electron Microscope (SEM) (SIGMA) microscope. Transmission Electron Microscopy (TEM), High Resolution Transmission Electron Microscopy (HR-TEM), Selected Area Electron Diffraction (SAED) and Energy Dispersive X-Ray Spectroscopy (EDX) measurements for FBNPs were performed on a JEOL JEM-2100 microscope.

3 Results and discussion

3.1 Synthesis and detection rationale

Scheme 1A depicts the synthetic route of core-shell FBNPs. The first step is the formation of Ag shell around the Au core. Adding CV, immediately followed by adding CS, produces Au@Ag@CS NPs. Au core provides higher chemical stability and durability to the whole material[15]. Furthermore, Au core causes fluorescence quenching and Raman enhancement of CV. But, the existence of metal shell would undermine the signals of the internal standards to some extent[40, 41], so rational control the thickness of Pt shell is of paramount importance. CS, a natural, biocompatible and nontoxic polysaccharide, is employed to prevent CV from detaching during the reaction. Without CS, the Raman signal of CV in the position of 591 cm^{-1} in the prepared FBNPs wouldn't be detected. On the contrary, obvious Raman signal of CV could be discovered in the FBNPs formed with the assistance of CS (Fig. S1). Meanwhile, the high zeta potential (+46.8 mV) imparted by CS proves the high stability of the NPs, because NPs with a zeta potential above (+30 mV) are generally considered to be stable in suspension[42]. Without CS, the FBNPs showed a strong tendency to agglomerate (Fig. S2). In addition, the positively charged property (+46.8 mV) due to the existence of $-NH3^+$ groups in CS under acidic conditions further enhances the peroxidase-like activity[8, 43, 44], because the positively charged property of NPs would influence the absorption of H_2O_2 and the particle-mediated electron transfer processes[8]. The conversion from Au@Ag@CS to FBNPs is achieved via the concerted actions of both the galvanic replacement of Ag by Pt through the addition of H_2PtCl_6 and AA reduction. The growth of Pt via galvanic replacement reaction is much faster than the reagent reduction process[45]. Ag structures on the Au surfaces are first dismantled by galvanic replacement of Ag by Pt and many

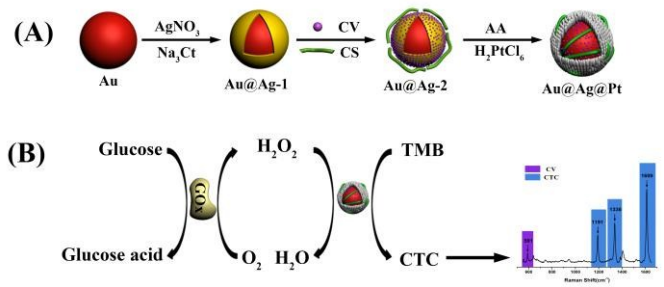

Scheme 1 Schematic for the synthesis of core-shell FBNPs (A) and the detection of glucose (B).

growth points for Pt form at the positions where Ag are located before. A smooth Ag shell accelerates the reaction rate and serves as a sacrificial template for the Pt coating. Without the involvement of Ag shell, the galvanic replacement of Ag by Pt wouldn't take place in time and the color of the solution didn't show obvious change until 4 hours later. The loading of Pt wasn't complete, either. The subsequent epitaxial growth of the Pt NPs attributes to the deposition of Pt atoms produced by reagent reduction onto the existing Pt structures. AA is a prerequisite for the formation of Pt multi-branches. Au@Pt NPs with a smooth Pt shell has been reported without using AA[46]. Our approach results in the growth of the ideal Pt multi-branches shell surrounding the Au@Ag core and the shell thickness can be tuned under our control by simply changing the amount of H_2PtCl_6.

The as-prepared NPs were characterized by a series of tests. Fig. 1A shows the UV-*vis* spectra of the original Au NPs, Au@Ag NPs and FBNPs. Au NPs exhibits an absorbance band at 525 nm. The observed new bands at 497 nm and 387 nm indicate the formation of Ag shell. However, when adding H_2PtCl_6 to the solution, the surface plasmon resonance (SPR) peak of the FBNPs shows a wider band, which may due to the following reasons [47]: The absorption band of the core could be influenced by the multi-branches of Pt shell, which has no characteristic absorption in UV-*vis* spectroscopy and would strongly damp out the dipolar plasmon oscillations of the Au core [20]. In addition, the change in the dielectric that surrounds the Au core may be a significant factor as well as the scattering by the Pt shell. Plus, the depletion of Ag layer is responsible for the change as well. Scanning electron microscopy (SEM) and transmission electron microscopy (TEM) images in Fig. 1B & C demonstrate the formation of the uniform and monodisperse FBNPs with an average diameter of 50 nm. The strong contrast revealed in the TEM image of a single particle clearly delineates the inner Au core surrounded by Pt multi-branches (the inset in Fig. 1D). In the high-resolution (HR)-TEM image (Fig. 1D), the observed lattice fringes (d=0.227 nm) corresponds to the (111) planes of Pt face-centered cubic (fcc) crystals [10]. Selected-area electron diffraction (SAED) patterns of the Pt shells (Fig. S3A) demonstrates the ring patterns with intense spots assigned to (111), (200), (220), and (311) plane of Pt fcc crystals [10], indicating the polycrystalline nature of Pt. Composition analysis by Energy Dispersive X-Ray Spectroscopy (EDX) spectroscopy (Fig. S3C) shows an Ag/Au molar ratio of 0.59: 1. Compared with the initial Ag/Au proportion (1.21: 1), the amounts of Ag decrease dramatically after the formation of FBNPs, which implies the galvanic replacement of Ag by Pt. With the increase of H_2PtCl_6, the amount of Ag tends to decline gradually (Fig. S3) and Pt multi-branches come into being by degrees (Fig. S4). A smooth Pt shell would be formed without AA [46], suggesting the irreplaceable reduction role of AA. All the characterization data conform to our suggested growth mechanism.

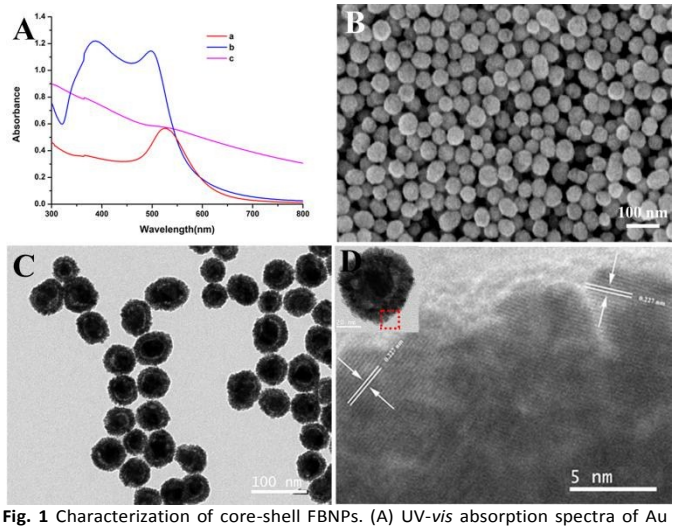

Fig. 1 Characterization of core-shell FBNPs. (A) UV-*vis* absorption spectra of Au NPs (a), Au@Ag NPs (b) and FBNPs (c). (B) SEM and (C) TEM images of FBNPs. (D) HR-TEM image of the Pt shell taken from the dashed region in the inset.

The universal H_2O_2-TMB catalytic system can be employed to detect H_2O_2 and the related substances. Glucose, for instance, can be measured utilizing this common platform. Concretely speaking, coupling the selective oxidation of glucose by GOx with the peroxidase-like activity of the FBNPs, the analysis of glucose can be carried out via detecting the RRS signal of charge transfer complex (CTC), which is shown in Scheme 1B. Unlike prior works, the present work took advantage of the high sensitivity of the RRS to analyze glucose instead of UV-*vis* spectroscopy. Furthermore, the potential signal fluctuations of RRS were corrected by the signals of internal standard molecules. This new type of biosensor does not require complex modification or enzyme immobilization. Our work provides a simple, sensitive and highly selective approach for glucose detection in serum.

3.2 Verification of the peroxidase-like activity of FBNPs

To assess whether FBNPs would exhibit peroxidase mimetic catalytic ability, we tested catalytic oxidation peroxidase substrates TMB in the presence of H_2O_2. As shown in the inset of Fig. 2A, TMB can be oxidized into a blue product in the presence of H_2O_2 and FBNPs. In contrast, the mixture of other substances didn't show characteristic color or only exhibit light blue color. Furthermore, UV-*vis* spectroscopy was used to characterize the different solutions. Fig. 2A shows that weak absorptions at 370 nm and 652 nm are observed in the case of other mixtures. A much stronger absorbance is observed in the presence of the FBNPs in a TMB and H_2O_2 solution, demonstrating that the reaction of TMB with H_2O_2 is hugely accelerated by the FBNPs, which means that the as-prepared FBNPs do encompass peroxidase-like activity. When using Au NPs and Au@Ag NPs as the catalysts, we can infer from Fig. S5: the peroxidase activity of Au NPs and Au@Ag NPs was negligible, which is in line with the reported works[8]. Even though the color of solution utilizing Au@Ag@CS NPs as catalysts was slighter deeper than employing Au NPs, Au@Ag NPs, which may owe to the positively charged property[8] of Au@Ag@CS NPs, its catalytic ability was still not comparable to FBNPs (Fig. S5). This certifies the pivotal role of Pt shell in enhancing the peroxidase activity of the whole nanoparticle.

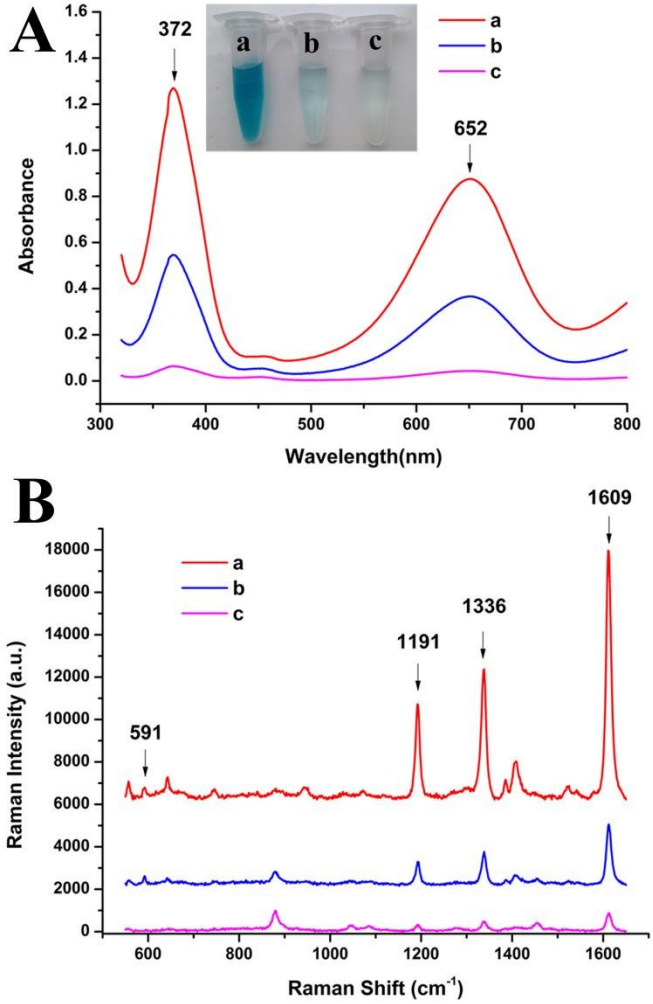

Fig. 2 (A) UV-*vis* absorption spectra and (B) Raman spectra of different reaction solutions, respectively. (a) TMB, H_2O_2 and FBNPs, (b) TMB and FBNPs, (c) TMB and H_2O_2. The inset in A shows the photograph of different reaction solutions.

The potential mechanism for this system is the radical chain reaction[48, 49], in which the oxygen-oxygen bond of H_2O_2 is rapidly broken by the catalytic action of Pt shell to give hydroxyl radicals. The resulting hydroxyl radicals were stabilized at the surface of the Pt shell, so it was the produced hydroxyl radicals that catalyzed TMB into CTC. The oxidation of TMB by H_2O_2 went through a two-step two-electron reaction[25] (Fig. S6). The blue product belonging to charge transfer complex (CTC) is attributed to the reversible complexation of the diamine and final diimine. We further characterized the peroxidase-like activity of the FBNPs through Raman spectroscopy (Fig. 2B). Raman bands assigned to CTC are summarized in Table S1. The analyses produced by Raman measurement consisted with UV-*vis* spectroscopy results. All of the results demonstrate that FBNPs possess peroxidase-like catalytic ability.

3.3 Optimization of the experimental parameters

The catalytic ability of the FBNPs depends on the amounts of H_2PtCl_6, pH and temperature. With the increase of H_2PtCl_6, also comes the enhancement of the catalytic performance of the FBNPs. However, this is at the expense of reducing the Raman signals of CV at 591 cm^{-1}, for the signals have to penetrate the thicker Pt shell to be detected, which is in line with some reported works[40, 41]. The signals of CV were strong enough to act as internal standards but the peroxidase-like activity of FBNPs was unsatisfying if we chose 1200 μL of H_2PtCl_6. When the amounts of H_2PtCl_6 were 2400 μL, the catalytic performance was amazing while the signals of CV were too weak to correct the potential fluctuations. With the purpose of obtaining a better catalytic performance and enabling the Raman signal of CV at 591 cm^{-1} to calibrate deviation, the optimal amounts of H_2PtCl_6 were 1800 μL (Fig. 3A). In order to reduce the reaction time, the influence of the amount of the FBNPs was observed as well. The Raman signal of CTC at 1609 cm^{-1} gradually increased until the amounts of the FBNPs reached 200 μL. Meanwhile, the Raman signal of CV at 591 cm^{-1} continued to increase slightly above 200 μL (Fig. 3B) for the concentration of CV increased with the adding of FBNPs. The signals of CV were fully capable of correcting the fluctuations when the amounts of FBNPs reached 200 μL. Thus, the best amounts of the FBNPs were 200 μL. We measured the peroxidase-like activity of the FBNPs while varying pH from 2 to 9, the temperature from 25°C to 60°C. As shown in Fig. 3C & D, the normalized Raman intensity, difference in band intensity of CTC at 1609 cm^{-1} between experimental sample and the control sample (0 μM of H_2O_2) divides the band intensity of the internal standard at 591 cm^{-1}, reached the maximum value at pH 4 and 45°C, respectively. Therefore, the optimal temperature and pH were approximately 45°C and pH 4, which were similar to the values for horseradish peroxidase (HRP)[1]. Compared with some previous works[31, 32], the optimal temperature for FBNPs was 45°C rather than room temperature. In our experiment, heating resulted in the stronger background signals as well. But, in a given time, the increase in Raman signals caused by the higher peroxidase-like activity of FBNPs was stronger than the increase derived from background signals (Fig. S7). Also, relatively long Raman accumulation times (10 s twice accumulations) were suitable

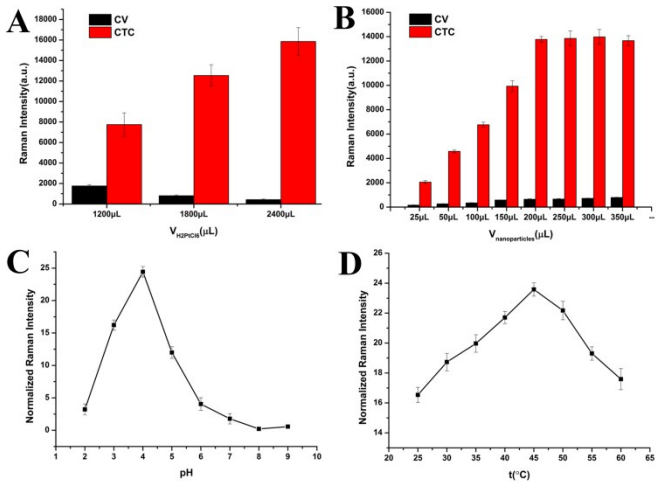

Fig. 3 Optimization of experimental conditions: (A) The amounts of H_2PtCl_6, (B) The amounts of FBNPs, (C) The pH of the reaction buffer, (D) The incubation temperature.

in our work to achieve more sensitive results.

3.4 Influence of H_2O_2 and TMB concentrations on reaction rate

To investigate the catalytic mechanism of the FBNPs, the apparent steady-state kinetic parameters were determined by changing the concentrations of TMB and H_2O_2, respectively. As shown in Fig. 4A & B, they share a common tendency that the reaction rate gradually increases until they reach the maximum. From Lineweaver-Burk plots of the double reciprocal of the Michaelis-Menten equation, we obtained the Michaelis-Menten constant (K_m) and maximum initial velocity (V_{max}). Relevant figures are displayed in Fig. 4C & D, and the results are summarized in Table S2. For enzymes, K_m demonstrates the affinity for the substrate. The smaller the value of K_m is, the more efficient the catalyst is, and the stronger the affinity between the enzyme and the substrate is[1]. The apparent of K_m value for the FBNPs with H_2O_2 as the substrates were lower than HRP[1], indicating that the FBNPs have a higher affinity for H_2O_2 than HRP[1].

3.5 Application of FBNPs in the detection of H_2O_2

Because the catalytic activity of the FBNPs is H_2O_2 concentration dependent, H_2O_2 can be detected in this way. Under the optimal conditions, the above-discussed method was used for H_2O_2 detection. As shown in Figure S8 (A), the normalized Raman intensity varies with a change of the concentration of H_2O_2, which presents a nearly exponential increasing curve in the tested concentration range. Fig. S8 (B) shows the linear relationship between the natural logarithm over the concentration of H_2O_2 ranging from 10 pM to 100 μM and the normalized Raman intensity. Compared with detecting H_2O_2 via UV-*vis* spectroscopy[8, 50] and chemiluminiscence[27, 51], the limit of detection is lower in our work thanks to the high sensitivity of RRS. Also, the obtained limit of detection for H_2O_2 is lower than our former work using RRS[29] as well because of the higher peroxidase activity of FBNPs. Besides, in comparison with our work referring to detection of melamine based on SERS and peroxidase mimetics[30], introduction of Pt NPs further enhances peroxidase-like activity; embedding the internal standard molecules (CV) corrects the potential fluctuations and guarantees signal reproducibility. In addition, the detection is faster, lower use of sample volume and simpler than those reported utilizing electrochemical method[52].

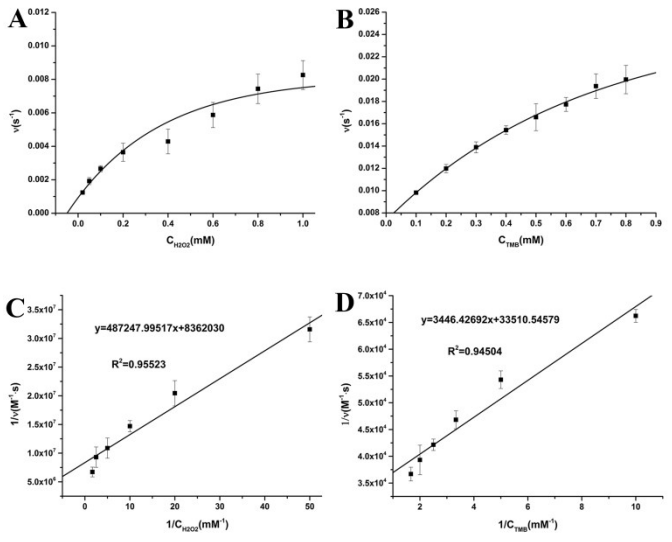

Fig. 4 Steady-state kinetic assay of FBNPs. The velocity (v) of the reaction was measured using 200 μL of FBNPs in 630 μL of 0.2 M acetate buffer (pH 4.0) and 45°C. The error bars represent the standard error derived from three separately prepared samples. (A) The concentration of TMB was 0.75 mM and H_2O_2 concentration was varied. (B) The concentration of H_2O_2 was 40 mM and TMB concentration was varied. (C, D) Double reciprocal plots of activity of FBNPs with the concentration of one substrate (TMB or H_2O_2) fixed and the other varied.

3.6 Application of FBNPs in the detection of glucose with high sensitivity and selectivity

Combining the catalytic reaction of TMB in the presence of GOx, the glucose detection could be readily carried out. Here, the background signal was removed from all spectra. Namely, the peak height at 1609 cm^{-1} for the control sample (0 μM of glucose) was subtracted from the peak height at 1609 cm^{-1} for each concentration of glucose. Fig. 5A displays that the normalized Raman intensity (after removing background signal, the peak intensity at 1609 cm^{-1} divided the band intensity of the internal standard at 591 cm^{-1}) exhibits a nearly exponential increasing curve as well. Fig. 5B shows the linear relationship between the natural logarithm over the concentration of glucose ranging from 1 nM to 200 μM. The general range of blood glucose concentration in healthy and diabetic persons is about 4.4-6.6 mM and 9-40 mM, respectively [53, 54]. Therefore, the proposed method is capable of quantitative detection of glucose in real samples with only requiring simple dilution. In addition, the limit of detection demonstrated taking advantage of Raman spectroscopy is lower than those reported using UV-*vis* spectroscopy measurements[8, 26, 50, 55] and chemiluminiscence[27, 51]. Furthermore, in comparison with

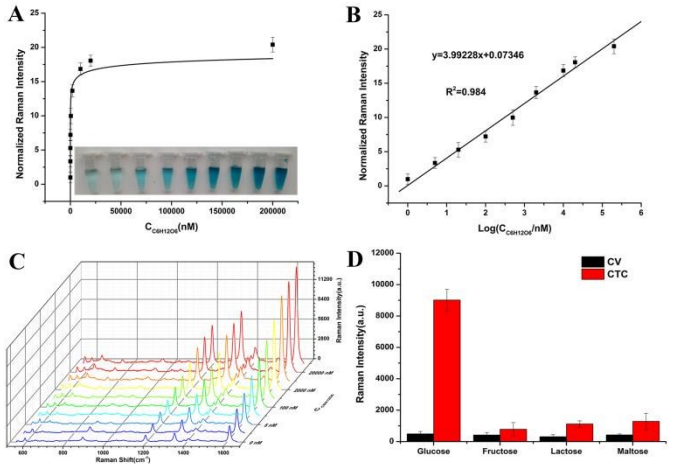

Fig. 5 (A) Glucose concentration dependant of normalized Raman intensity. The inset shows the color change for different concentrations of targets. (B) The calibration curve of normalized Raman intensity against natural logarithm over concentration of glucose. (C) Raman spectra of the solutions with different concentrations of targets. (D) The selectivity of the proposed method towards glucose detection. The error bars illustrate the standard deviations of three separately prepared samples.

electrochemical method, this type of sensor is rapid, convenient and reliable. Admittedly, glucose sensing has been realized with the help of GOx to modify electrodes, but the immobilization of enzymes on solid interfaces is commonly considered in order to improve the long-term and operational stability of enzymes and this is often at the expense of significant loss in the catalytic activity of the enzymes[52]. With the purpose of addressing the limitations of enzyme, scientists have devoted to nonenzymetic sensors. Although the problem of insufficient long-term stability has been solved, the adsorption of oxidation intermediates of glucose or active species in the solution may significantly block the electrode activity for direct electro-oxidation of glucose[56]. Besides, nonenzymatic sensors offer analytical selectivity inferior to the enzymatic sensors[57].

Considering that the existence of some potential interfering substances, such as fructose, lactose, and maltose, might affect the detection of glucose in analysis, the selectivity of this method was investigated. As shown in Fig. 5D, even when the concentrations of the control samples are 10 times larger than that of glucose, no obvious response is observed, indicating that the proposed method can be used to detect glucose selectively.

The general range of blood glucose concentration in healthy and diabetic persons is about 3-8 mM[26] and 9-40 mM, respectively[53, 54]. Therefore, the proposed method is capable of quantitative detection of glucose in real samples with only requiring simple dilution. For glucose detection in serum, the samples were first diluted 100-fold by PBS, the concentration of glucose in the normal serum sample is about 4.90 mM according to the calibration curve. When the glucose concentration is deviant, we can detect it easily employing this system, which implies that this method is able to determine glucose in real samples.

3.7 Application in real samples

To further confirm the reliability of the proposed method in practical applications, the detection of glucose in human serum samples was also conducted. The blood samples were firstly diluted 100-fold by PBS before determination. Certain amounts of glucose were spiked in the samples. The final results are summarized in Table S3. The recoveries of the real samples are in the range of 94.8-102.3% with the relative standard deviation of 1.84-4.52%. The desirable results clearly demonstrated the feasibility of the proposed method for determination of glucose in real samples.

Conclusions

In summary, FBNPs can be prepared conveniently via the concerted actions of both galvanic replacement and reagent reaction. The FBNPs possess highly intrinsic peroxidase-like activity owing to the formation of Frucus Broussonetiae-shaped Pt shell, the absence of surfactants and the positively charged CS molecules intertwined within the outermost Pt NPs. The preformed Au@Ag NPs act as template and guarantee the uniformity of the final products. Afterwards, the epitaxial growth of Pt multi-branches can be realized at room temperature without the participation of any surfactant. The internal standard molecules, cresyl violet (CV), play the role of correcting the potential fluctuations. CS is used to prevent the CV from detaching, protect the nanostructures, and further enhance the peroxidase-like activity of the FBNPs. Taking advantage of the high sensitivity of resonance-enhanced Raman spectroscopy (RRS) and the high catalytic ability of the FBNPs, H_2O_2 and glucose can be detected with broader ranges from 10 pM to 100 μM, and from 1 nM to 200 μM, respectively. We think this work is suitable for biochemistry and clinical diagnosis

Acknowledgements

This work was financially supported by National Natural Science Foundation of China (Nos. 21175101, 21475100 and 81471696), Foundation of China Geological Survey (No. 12120113015200), and Natural Science Foundation of Hubei Province of China (No. 2014CFA002)

Notes and references

1 L. Gao, J. Zhuang, L. Nie, J. Zhang, Y. Zhang, N. Gu, T. Wang, J. Feng, D. Yang, S. Perrett and X. Yan, *Nat. Nanotechnol.*, 2007, **2**, 577-583.
2 X.-R. Li, M.-C. Xu, H.-Y. Chen and J.-J. Xu, *J. Mater. Chem. B*, 2015, **3**, 4355-4362.
3 Y. Fan, W. Shi, X. Zhang and Y. Huang, *J. Mater. Chem. A*, 2014, **2**, 2482-2486.
4 J. Hao, Z. Zhang, W. Yang, B. Lu, X. Ke, B. Zhang and J. Tang, *J. Mater. Chem. A*, 2013, **1**, 4352-4357.
5 C. Ray, S. Dutta, S. Sarkar, R. Sahoo, A. Roy and T. Pal, *J. Mater. Chem. B*, 2014, **2**, 6097-6105.
6 X. Chen, N. Zhai, J. H. Snyder, Q. Chen, P. Liu, L. Jin, Q. Zheng, F. Lin, J. Hu and H. Zhou, *Anal. Methods*, 2015, **7**, 1951-1957.
7 J. Guan, J. Peng and X. Jin, *Anal. Methods*, 2015, **7**, 5454-5461.
8 Y. Jv, B. Li and R. Cao, *Chem. Commun.*, 2010, **46**, 8017-8019.
9 W. He, Y. Liu, J. Yuan, J. J. Yin, X. Wu, X. Hu, K. Zhang, J. Liu, C. Chen, Y. Ji and Y. Guo, *Biomaterials*, 2011, **32**, 1139-1147.
10 H. Ataee-Esfahani, L. Wang, Y. Nemoto and Y. Yamauchi, *Chem. Mater.*, 2010, **22**, 6310-6318.
11 Y. Feng, H. Liu and J. Yang, *J. Mater. Chem. A*, 2014, **2**, 6130-6137.
12 C. Zheng, A.-X. Zheng, B. Liu, X.-L. Zhang, Y. He, J. Li, H.-H. Yang and G. Chen, *Chem. Commun.*, 2014, **50**, 13103-13106.
13 A. Higuchi, Y.-D. Siao, S.-T. Yang, P.-V. Hsieh, H. Fukushima, Y. Chang, R.-C. Ruaan and W.-Y. Chen, *Anal. Chem.*, 2008, **80**, 6580-6586.
14 G.-W. Wu, S.-B. He, H.-P. Peng, H.-H. Deng, A.-L. Liu, X.-H. Lin, X.-H. Xia and W. Chen, *Anal. Chem.*, 2014, **86**, 10955-10960.
15 H. Li, H. Wu, Y. Zhai, X. Xu and Y. Jin, *ACS Catal.*, 2013, **3**, 2045-2051.
16 H. You, F. Zhang, Z. Liu and J. Fang, *ACS Catal.*, 2014, **4**, 2829-2835.
17 J. Liu, X. Hu, S. Hou, T. Wen, W. Liu, X. Zhu, J.-J. Yin and X. Wu, *Sens. Actuators B*, 2012, **166**, 708-714.
18 W. He, X. Wu, J. Liu, X. Hu, K. Zhang, S. Hou, W. Zhou and S. Xie, *Chem. Mater.*, 2010, **22**, 2988-2994.

19 S. Guo, L. Wang, S. Dong and E. Wang, *Chem. Mater.*, 2008, **112**, 13510-13515.
20 S. Guo, J. Li, S. Dong and E. Wang, *Chem. Mater.*, 2010, **114**, 15337-15342.
21 H. M. Song, D. H. Anjum, R. Sougrat, M. N. Hedhili and N. M. Khashab, *J. Mater. Chem.*, 2012, **22**, 25003-25010.
22 P. Song, L.-L. He, A.-J. Wang, L.-P. Mei, J. Chen and J.-J. Feng, *J. Mater. Chem. A*, 2015, **3**, 5321-5327.
23 J. J. Wang, D. X. Han, X. H. Wang, B. Qi and M. S. Zhao, *Biosens. Bioelectron.*, 2012, **36**, 18-21.
24 N. Ding, N. Yan, C. Ren and X. Chen, *Anal. Chem.*, 2010, **82**, 5897-5899.
25 S. Laing, A. Hernandez-Santana, J. r. Sassmannshausen, D. L. Asquith, I. B. McInnes, K. Faulds and D. Graham, *Anal. Chem.*, 2010, **83**, 297-302.
26 Y. Song, K. Qu, C. Zhao, J. Ren and X. Qu, *Adv. Mater.*, 2010, **22**, 2206-2210.
27 W. Shi, X. Zhang, S. He and Y. Huang, *Chem. Commun.*, 2011, **47**, 10785-10787.
28 Y. Wang, B. Yan and L. Chen, *Chem. Rev.*, 2012, **113**, 1391-1428.
29 L. Wang, A. Shen, X. Li, Y. Zeng, X. Zhou, R. M. Richards and J. Hu, *RSC Adv.*, 2014, **4**, 34294-34302.
30 J. Li, G. Zhang, L. Wang, A. Shen and J. Hu, *Talanta*, 2015, **140**, 204-211.
31 K. S. McKeating, S. Sloan-Dennison, D. Graham and K. Faulds, *Analyst*, 2013, **138**, 6347-6353.
32 Z. Yu, Y. Park, L. Chen, B. Zhao, Y. M. Jung and Q. Cong, *ACS Appl. Mater. Interfaces*, 2015, **7**, 23472-23480.
33 P. J. Aarnoutse and J. A. Westerhuis, *Anal. Chem.*, 2005, **77**, 1228-1236.
34 S. O. Konorov, H. G. Schulze, M. W. Blades and R. F. B. Turner, *Anal. Chem.*, 2014, **86**, 9399-9404.
35 A. Lorén, J. Engelbrektsson, C. Eliasson, M. Josefson, J. Abrahamsson, M. Johansson and K. Abrahamsson, *Anal. Chem.*, 2004, **76**, 7391-7395.
36 S. E. J. Bell and N. M. S. Sirimuthu, *Chem. Soc. Rev.*, 2008, **37**, 1012-1024.
37 W. Shen, X. Lin, C. Jiang, C. Li, H. Lin, J. Huang, S. Wang, G. Liu, X. Yan, Q. Zhong and B. Ren, *Angew. Chem. Int. Ed.*, 2015, **54**, 7308-7312.
38 W. Xie, L. Su, P. Donfack, A. Shen, X. Zhou, M. Sackmann, A. Materny and J. Hu, *Chem. Commun.*, 2009, 5263-5265.
39 A. G. Shen, L. F. Chen, W. Xie, J. C. Hu, A. Zeng, R. Richards and J. M. Hu, *Adv. Funct. Mater.*, 2010, **20**, 969-975.
40 P. Zhang and Y. Guo, *J. Am. Chem. Soc.*, 2009, **131**, 3808-3809.
41 D. K. Lim, K. S. Jeon, J. H. Hwang, H. Kim, S. Kwon, Y. D. Suh and J. M. Nam, *Nat. Nanotechnol.*, 2011, **6**, 452-460.
42 G. Sonavane, K. Tomoda and K. Makino, *Colloids Surf. B*, 2008, **66**, 274-280.
43 Y. F. Zhang, C. L. Xu, B. X. Li and Y. B. Li, *Biosens. Bioelectron.*, 2013, **43**, 205-210.
44 X.-X. Wang, Q. Wu, Z. Shan and Q.-M. Huang, *Biosens. Bioelectron.*, 2011, **26**, 3614-3619.
45 W. Xie, C. Herrmann, K. Kömpe, M. Haase and S. Schlücker, *J. Am. Chem. Soc.*, 2011, **133**, 19302-19305.
46 L. Kuai, S. Wang and B. Geng, *Chem. Commun.*, 2011, **47**, 6093-6095.
47 Z. L. Liu, B. Zhao, C. L. Guo, Y. J. Sun, F. G. Xu, H. B. Yang and Z. Li, *J. Phys. Chem. C*, 2009, **113**, 16766-16771.
48 M. Ma, Y. Zhang and N. Gu, *Colloids Surf. A*, 2011, **373**, 6-10.
49 A. Harriman, G. R. Millward, P. Neta, M. C. Richoux and J. M. Thomas, *J. Phys. Chem.*, 1988, **92**, 1286-1290.
50 H. Wei and E. Wang, *Anal. Chem.*, 2008, **80**, 2250-2254.
51 Y. Fan and Y. Huang, *Analyst*, 2012, **137**, 1225-1231.
52 V. Urbanova, M. Magro, A. Gedanken, D. Baratella, F. Vianello and R. Zboril, *Chem. Mater.*, 2014, **26**, 6653-6673.
53 R. Badugu, J. R. Lakowicz and C. D. Geddes, *Analytical Chemistry*, 2004, **76**, 610-618.
54 P. Wu, Y. He, H.-F. Wang and X.-P. Yan, *Anal. Chem.*, 2010, **82**, 1427-1433.
55 Q. Chen, M. Liu, H. Li, Y. Zhang and S. Yao, *Chem. Commun.*, 2014, **50**, 6771-6774.
56 C. Chen, Q. Xie, D. Yang, H. Xiao, Y. Fu, Y. Tan and S. Yao, *RSC Adv.*, 2013, **3**, 4473-4491.
57 D. W. Kimmel, G. LeBlanc, M. E. Meschievitz and D. E. Cliffel, *Anal. Chem.*, 2012, **84**, 685-707.

Core-shell Fructus Broussonetiae-like Au@Ag@Pt nanoparticles as highly efficient peroxidase mimetics for supersensitive resonance-enhanced Raman sensing

Junrong Li, Liang Lv, Guannan Zhang, Xiaodong Zhou, Aiguo Shen* and Jiming Hu*

We herein present a simple and surfactant-free synthetic strategy to prepare core-shell Fructus Broussonetiae-like Au@Ag@Pt nanoparticles (FBNPs) via concerted actions of both galvanic replacement and reagent reduction, in which the chitosan (CS)-mediated epitaxial growth of Pt multi-branches occurs on the cresyl violet (CV) labeled Au core Ag shell nanoparticles (NPs) at room temperature. The as-prepared novel nanostructures possess intriguing enzyme mimetic activity due to the formation of Frucus Broussonetiae-shaped Pt shell, the absence of surfactants and the positively charged CS molecules intertwined within the outermost Pt NPs. Relying on the high sensitivity of resonance-enhanced Raman scattering (RRS) and the highly efficient intrinsic peroxidase-like activity of FBNPs, H_2O_2 was detected with a wider detection window from 10 pM to 100 μM when utilizing 3, 3', 5, 5'-tetramethylbenzidine (TMB) as substrates. It is exactly based on a H_2O_2-TMB catalytic oxidation system that a simple, sensitive, selective and universal platform has been reasonably extended for detection of all peroxidase-related analytes. Glucose with a concentration range (1 nM-200 μM), for example, has been detected in the presence of glucose oxidase (GOx) with a limit of detection of 1 nM.